

Abstract High energy single- to few-cycle terahertz pulses enable the exploration of the frontier of science, such as electron acceleration, strong-field physics, and spectroscopy. One important method of generating such terahertz pulses is to use the tilted-pulse-front (TPF) technique. However, due to the non-collinear phase-matching, the large angular dispersion leads to a spatial and temporal break-up of the optical pump, limiting the terahertz generation efficiency and reducing the few-cycle character of the generated terahertz fields. To reduce the effects caused by angular dispersion, multiple schemes with discrete pulse-front-tilt have been suggested. We propose a terahertz generation scheme, where a spatio-temporally chirped (STC) pump pulse is utilized. With our 2D+1 numerical model, we perform a systematic comparative study of the conventional TPF scheme, three discrete TPF schemes, and the STC scheme. This model predicts smaller optimal interaction length and significantly smaller conversion efficiency compared to simple 1D models. We conclude that the STC scheme delivers spatially homogeneous few-cycle terahertz pulses with the highest conversion efficiency. Additionally, given a short interaction length, the discrete TPF schemes cannot outperform the continuous ones. In general, this work gives guidance to choose the most appropriate setup for a given terahertz experiment.

Tilted-pulse-front schemes for terahertz generation

Lu Wang^{1,2,*}, György Tóth³, János Hebling^{3,4,5} and Franz Kärtner^{1,2,6}

1. Introduction

The last several decades have witnessed a tremendous increase in the laser-based, high-energy terahertz applications [1] such as spectroscopy [2], strong field terahertz physics [3, 4], particle acceleration [5], electron spin manipulation [3] and phonon resonance studies [6]. Optical rectification is an important method for terahertz generation, where an ultrashort pump laser pulse induces a strong dipole moment via the second-order nonlinear effect. During the interaction of the terahertz and the optical beams, a repeated energy down conversion of pump photons (cascading effect) is possible, leading to broadband terahertz pulse emission with an efficiency close to, or even above, the Manley-Rowe limit [7]. The "tilted-pulse-front" (TPF) technique, a phase matching (PM) method for terahertz generation by optical rectification, or more generally for a non-collinear interaction, brings new possibilities to generate high energy terahertz pulses. In this technique, the intensity front of the optical pump (OP) is tilted with respect to the phase front [8]. The generated terahertz propagates perpendicularly to the TPF [9]. Due to the non-collinear phase-matching, frequency downshifted optical components generated via the cascading effect, possess large angular spread. This leads to a spatial and temporal break-up of the optical pump, limiting the terahertz generation efficiency and reducing the few-cycle character of the generated terahertz fields. Furthermore, due to the material absorption at terahertz frequencies, limited damage threshold of the nonlinear material and the low terahertz photon to pump photon energy ratio, generating high energy terahertz pulses is challenging.

Multiple schemes have been suggested to generate pulse-front-tilt. In this article, we focus on two types of pulse-front-

tilt: "continuous", where the TPF forms a continuous plane and "discrete", where the TPF is achieved by discrete beamlet structure. The conventional grating (CG) scheme was proposed and demonstrated in 2002 by J. Hebling et.al. [9], where a diffraction grating induces angular dispersion onto the optical pump pulse, leading to a pulse front tilt. Shortly after, in 2004, the pulse front tilt caused by spatio-temporal chirp (STC) was proposed by S. Akturk et.al. [10]. In this case, the pulse front tilt is generated by propagating a transversely linear-chirped optical pulse through a dispersive medium. In this method, no angular dispersion occurs. However, this method has not been used to generate terahertz pulses. In 2016, B.K. Ofori-Okai et.al. [11] demonstrated a setup consisting of a stair-step reflective echelon (RES) structure instead of a reflective optical grating. The echelon produces a discretely tilted pulse front, decreasing the negative effect of large angular dispersion [11]. In 2017, a multistep phase mask (MSPD) scheme was proposed by Y. Avetisyan et.al. [12]. This scheme splits a single input beam into many smaller time-delayed "beamlets". Compared with the grating method, it decreases the negative effects of the angular dispersion and eliminates the necessity of the imaging optics. In the same year, L. Pálfalvi et.al. performed numerical studies of a nonlinear echelon (NLES) slab [13], where a stair-step echelon-faced nonlinear crystal is used instead of a nonlinear prism. It is expected that this scheme produces good-quality, symmetric terahertz beams. Recently, the corresponding experiment was demonstrated by P.S. Nugraha et.al. in 2019 [14]. The CG and STC schemes generate continuous TPF whereas the RES, MSPM and NLES schemes generate discrete TPF.

In this article, a 2-D+1 (x, z, t) numerical model is used to investigate the effectiveness of the various tilted pulse front

¹ Center for Free Electron Laser Science (CFEL), Deutsches Elektronen-Synchrotron, Hamburg, 22607, Germany ² Universität Hamburg, Department of Physics, Hamburg, 22761, Germany ³ University of Pécs, Institute of Physics, 7624 Pécs, Hungary ⁴ MTA-PTE High-Field Terahertz Research Group, 7624 Pécs, Hungary ⁵ University of Pécs, Szentágotthai Research Centre, 7624 Pécs, Hungary ⁶ The Hamburg Centre for Ultrafast Imaging (CUI), Hamburg, 22761, Germany

* Corresponding author: e-mail: lu.wang@desy.de

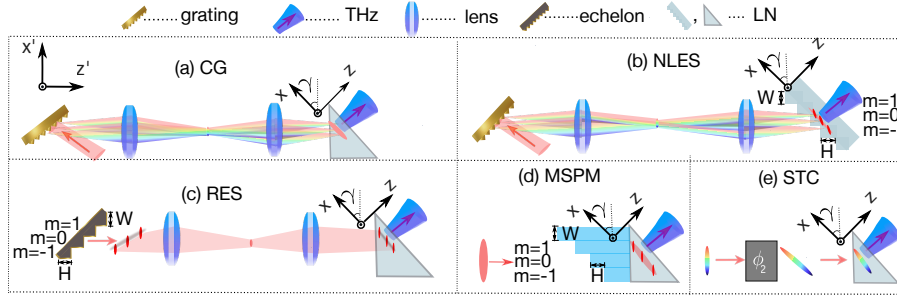


Figure 1 Schematic drawings of different tilted-pulse-front schemes. (a-e) are the configurations for conventional grating (CG), nonlinear echelon (NLES), reflective echelon (RES), multistep phase mask (MSPD) and spatio-temporal chirp (STC) schemes respectively. (b-d) represent the discrete TPF schemes whereas (a) and (e) represent the continuous TPF schemes. The step numbers of the structures are labeled by m . The apex of the LN crystal is located at $x = 0$. The $z=0$ coordinate is defined at the location where the center of the OP starts to interact with the LN crystal.

schemes. The effect of the vertical dimension (y dimension in Fig. 1) is of minor importance in this study [15]. The nonlinear material lithium niobate (LN) is chosen due to its large second order optical nonlinearity. The conversion efficiency and the spatial distribution of the generated terahertz electric fields are presented for the aforementioned 5 schemes. With thorough discussions of the advantages and disadvantages of each scheme, this work gives guidance to choose the most appropriate setup for a given terahertz experiment.

2. The investigated setups

The illustrations for different tilted-pulse-front schemes are presented in Fig. 1. For a fair comparison, the OP peak fluence, the OP beam size σ'_x and the size of the beamlets at the LN input surface (i.e after the optical elements and the imaging system) are set the same for all the schemes. The OP propagates along the z' direction and the terahertz propagates along the z direction. The analytical forms of the OP electric fields inside the LN crystal and the second order nonlinear polarisation can be found in the supporting information.

In schemes (a-c) in Fig. 1, the imaging systems are chosen such that the image of the grating (echelon) overlaps with the tilted pulse front inside the LN crystal [16]. This is considered to be the optimal imaging condition and the analytical expressions can be found in Eqs. (1-3) of the supporting information. The first lens has a fixed focal length $f_1 = 300$ mm and the second one, close to the LN, has a focal length f_2 . In scheme (e), the TPF is achieved by applying second-order dispersion ϕ_2 to a spatially chirped OP. Consequently, no initial angular dispersion is induced. The simulation parameters are listed in Table 1.

3. Results

3.1. Efficiency

Two OP beam sizes, 0.5 mm and 4 mm, corresponding to short and long interaction lengths are analyzed. The two

Table 1 Simulation parameters

parameter name	value
wavelength λ_0	1018 nm
beam size σ'_x	0.5 mm & 4 mm
grating period d	1/1500 mm
focal length f_1	300 mm
phase matching angle γ	64.8°
phase matching frequency Ω_0	$2\pi \times 0.3$ THz
pulse duration (FWHM) τ_0	500 fs [17]
temperature	300 K
peak fluence	$\sqrt{10\tau_0(\text{fs})}$ mJ/cm ² [18]
THz absorption (300K, 0.3 THz)	7/cm [19]
NLES scheme W, H	97 μm , 206 μm
RES scheme W, H	150 μm [11], 229 μm
MSPM scheme W, H	97 μm , 1000 μm
STC scheme ϕ_2	0.045 ps ²

beam sizes are chosen to elucidate the impact of upfront angular dispersion in connection with the short and longer interaction lengths, by solving the 2D+1 coupled nonlinear wave equations [15]. It can be seen in Fig. 2 that the CG scheme loses its advantage for longer interaction length, due to the maximum initial angular dispersion among all the 5 scheme. For the NLES scheme with high input OP fluence, the optimal effective length is $L_{\text{eff}} \approx 1/\alpha$. When $\sigma'_x > \sin(\gamma)L_{\text{eff}}$, the efficiency and the optimal interaction length is nearly independent of the OP beam size. Since the NLES slab creates beamlets at the LN input surface, all of the beamlets experience an almost identical condition i.e similar walk-off distance. Thus, the generated terahertz pulse properties are not related to the OP beam size, which is the unique character of the NLES scheme compared to all the other schemes.

The RES and the MSPM schemes are similar from the point of view that the PM is achieved entirely by generating time-delayed beamlets. However, despite the similar interaction length, RES outperforms MSPM in terms of efficiency due to the imaging system and the absence of dis-

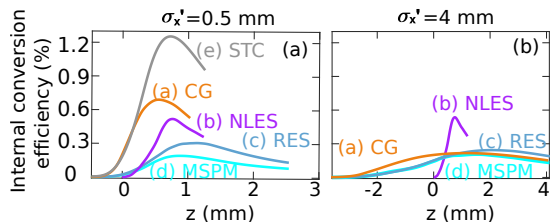


Figure 2 The internal conversion efficiency (without out-coupling loss) of different tilted-pulse-front schemes versus the interaction length (z). (a) and (b) correspond to 0.5 mm and 4 mm OP beam sizes respectively. The $z = 0$ coordinate is defined at the location where the center of the OP starts to interact with the LN crystal.

person in the mask material. In the MSPM scheme, the OP experiences diffraction and dispersion which modifies the spatial and temporal profiles of the beamlets (see Fig. 3(d)). The STC scheme delivers the highest conversion efficiency, since the OP contains zero initial angular dispersion and continuous TPF. However, the STC scheme is only applicable for a small OP beam size due to the limitation in OP bandwidth (see section 4, scheme (e) for more detail).

One can see that for the discrete TPF schemes (NLES, RES, MSPM), the conversion efficiency does not strongly depend on the OP beam size (or interaction length). With a short interaction length, the conversion efficiency of the discrete TPF schemes can not exceed the continuous TPF schemes. Since the beamlet structure leads to a discrete PM condition i.e the entire arrangement (envelope) of the beamlets forms the TPF, while each individual beamlet itself has an offset with respect to the perfect pulse-front-tilt surface (see supporting information). Additionally, among all the 3 discrete TPF schemes, the NLES scheme delivers the highest conversion efficiency since the beamlets are more tilted towards the pulse-front-tilt surface.

Figure 3 shows the impact of angular dispersion onto the OP. The initial angular dispersion condition of the 5 schemes is $CG > NLES > RES, MSPM > STC$. Figure 3(f-j)

suggest that with a given propagation distance, the OP with larger initial angular dispersion suffers more from temporal and spatial pulse break-up. This spatial and temporal break-up limits the terahertz generation efficiency and reduces the few-cycle character of the generated terahertz fields (see Fig. 4 for details).

3.2. Terahertz out-coupling loss

Due to the large terahertz refractive index inside LN ($n(\Omega_0) = 5.2$), a significant energy loss of the terahertz pulse propagating from the LN into the air is inevitable. The maximum Fresnel transmission T at the desired terahertz frequency is only $T = 1 - (n(\Omega_0) - 1)^2 / (n(\Omega_0) + 1)^2 = 0.54$. However, because of the distortion of the terahertz beams, T is much smaller and is very sensitive to the spatial distribution of the terahertz beam, which is largely dependent on the fluence and size of the OP. The T at the peak of each efficiency curve in Fig. 2 are calculated and the corresponding results are listed in Table 2.

For all the mentioned schemes apart from NLES, the terahertz fields, generated by OP with lower fluence or smaller beam size, express less spatial inhomogeneity and thus have higher transmission. Besides, larger OP beam size leads to lower terahertz frequency due to longer interaction length, since the absorption of the LN increases with the terahertz frequency (see supporting information). In principle, larger beam size would reduce the angular divergence and thus enhances the transmission. However, increasing the OP beam size does not lead to a strong increase of the terahertz beam size (see Fig. 4). Additionally, the resulting larger terahertz beam has worse beam quality due to the variation of interaction length along the transverse dimension x' caused by the prism geometry. On the other hand, one can see from Table 2 that the NLES scheme has the highest transmission (especially for large OP beams) owing to the spatially homogeneous terahertz beam quality.

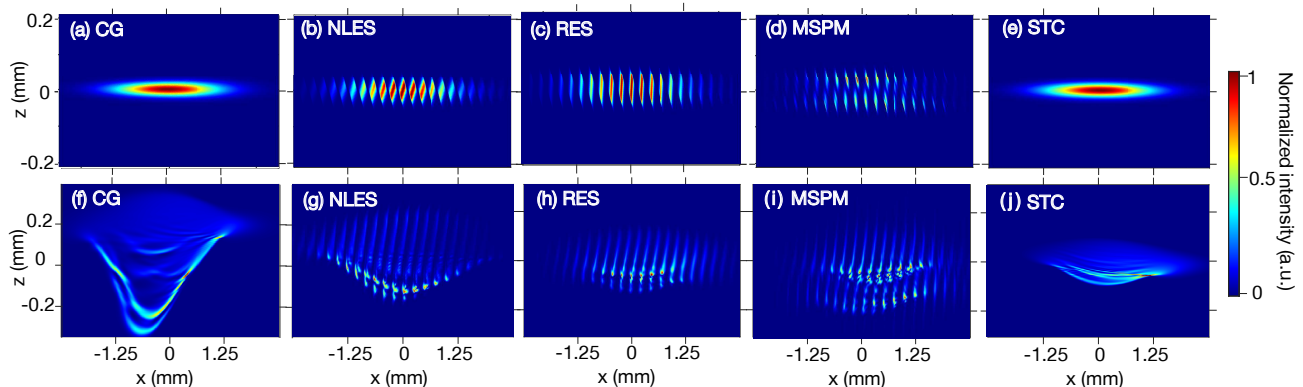


Figure 3 The OP ($\sigma_x' = 0.5$ mm) intensity distributions versus the transverse dimension x for different TPF schemes are shown. (a-e) show the corresponding input OP intensity distributions at the LN input surface. (f-j) show the corresponding OP intensity distributions after a given propagation distance (1.2 mm). The intensity distributions are shown in x - z coordinates where the distribution along z dimension is linearly related to the distribution in time and $\sigma_x = \sigma_x' / \cos(\gamma)$. The center of the OP is chosen to be $x = 0, z = 0$, for convince of representation.

Table 2 Terahertz energy transmission (T) and the external conversion efficiency (η_e) at the LN output surface. The highest η_e for a given OP beam size is marked by a black box.

	$\sigma'_x = 0.5$ mm		$\sigma'_x = 4$ mm	
	T	η_e (%)	T	η_e (%)
(a) CG	0.19	0.12	0.24	0.05
(b) NLES	0.46	0.24	0.53	0.29
(c) RES	0.34	0.11	0.29	0.07
(d) MSPM	0.31	0.06	0.27	0.06
(e) STC	0.39	0.48	-	-

4. Analyses of each scheme

To further understand the terahertz generation process with the aforementioned schemes, the terahertz electric fields at the peak of the efficiency curves in Fig. 2, generated by 0.5 mm and 4 mm OP beam sizes are presented in the following sections. Within the $x' - z'$ plane, two phase matching conditions need to be satisfied, in order to generate terahertz pulses efficiently (see derivation of PM conditions in the supporting information). One is shown in Eq.(1), where n_g is the group velocity refractive index of the LN at center frequency ω_0 and γ is the TPF angle. This condition ensures

that the projection of the pump velocity equals to the terahertz velocity [9]. This is also known as velocity matching, which applies to all the schemes discussed.

$$n(\Omega_0) \cos(\gamma) = n_g, \quad (1)$$

The other PM condition varies according to the scheme and is given in the following sections respectively. This condition is responsible for creating tilted (average) pump intensity front with the appropriate tilt angle γ .

Scheme (a): conventional grating (CG).

The ease of this setup, the high pulse energies and the controllability of the terahertz properties has made this scheme a strong candidate for generating high energy terahertz pulses approaching the millijoule range [20]. However, the transversal asymmetry of the interaction, in combination with the cascading effect, result in terahertz beams with non-uniform spatial distributions. The CG scheme utilizes the grating induced angular dispersion to form a pulse front tilt [8]. The angular dispersion has two effects on the OP away from the imaging plane i.e increase the OP pulse duration and decrease the TPF angle [21]. These two effects are more pronounced for larger angular dispersion (or broadband OP), leading to the minimum interaction length in the CG

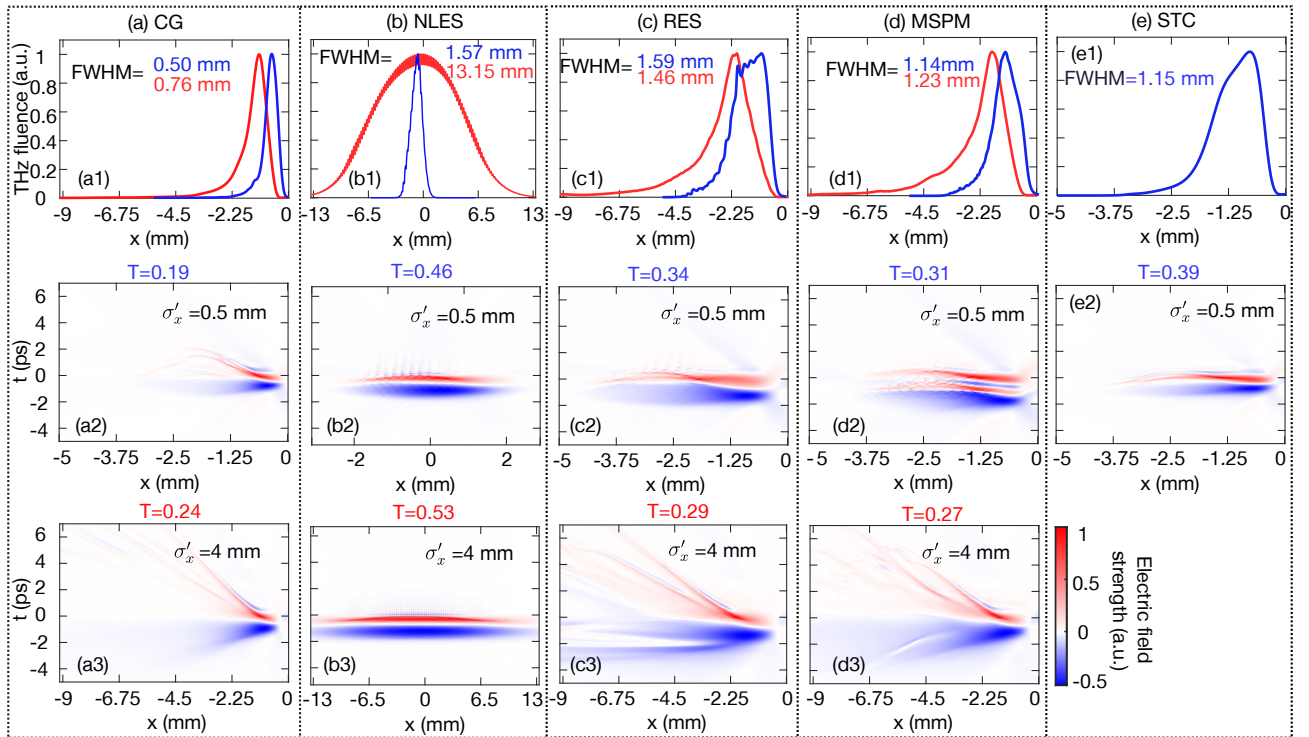


Figure 4 Numerical results of the terahertz electric fields generated by different schemes at the peak of the efficiency curves in Fig. 2 are shown. The LN apex is located at $x = 0$. The figure labels a-e correspond to schemes (a)-(e), respectively. (a1-e1) represent the output terahertz fluence with OP beam sizes 0.5 mm (blue) and 4 mm (red) respectively. The terahertz electric field distributions versus x generated by 0.5 mm and 4 mm OP are shown in (a2-e2) and (a3-d3) respectively. The terahertz energy transmission at the exit surface of the LN is denoted by T.

scheme compared with all the other schemes. The PM condition is given by Eq. (2), where c is the speed of light, $\beta = 2\pi/[\omega_0 \cos(\theta_o)d]$ is the first order angular dispersion induced by the grating and θ_o is the grating output angle.

$$\tan(\gamma) = \beta c f_1 / (f_2 n_g) \quad (2)$$

Fig. 4(a1-a3) indicate that, compared to the 0.5 mm OP, the terahertz field generated by 4 mm OP suffers from more transversal spread in terms of fluence and temporal distribution. Furthermore, most of the terahertz energy is contained in the single-cycle region of the terahertz electric field. By increasing the OP spot size by $\times 8$, the terahertz beam size increases only by 50%. This is the main reason of the efficiency drop for large OP beam size as shown in Fig. 2.

Scheme (b): nonlinear echelon (NLES).

This method is beneficial for generating high energy, large size and spatially homogeneous terahertz beams. The step size of the LN nonlinear echelon along the x' and z' dimensions are represented by W and H respectively (see Fig. 1(b)). The PM condition is given by

$$[n_g \tan(\gamma) - c\beta f_1 / f_2] W = H(n_g - 1) \quad (3)$$

In order to ensure that the terahertz pulse propagates perpendicular to the entrance and exit surfaces of the plan-parallel LN slab, the condition $H/W = \tan(\gamma)$ need to be satisfied [13]. With this condition, Eq. (3) reduces to $\tan(\gamma) = c\beta f_1 / f_2$. Compared with the CG scheme in Eq. (2), the NLES scheme requires less angular dispersion. Additionally, with different input OP pulse duration, the optimal effective length may differ. Thus, the thickness of the NLES slab should vary accordingly. However, for a given NLES with fixed thickness, this can be adjusted by adapting the pump fluence.

It can be seen from Fig. 4(b1-b3) that by changing the OP beam size the generated terahertz beam size changes accordingly. Besides, as long as $\sigma'_x > \sin(\gamma)L_{\text{eff}}$ is satisfied, the terahertz generation efficiency and the terahertz spectra are independent of the OP beam size, which is a unique property of this scheme. This property enables the possibility of generating high energy terahertz pulses by simply increasing the pump energy and the OP beam size. Additionally, the electric fields show strong single-cycle character homogeneously along the entire transverse dimension x .

Scheme (c): reflective echelon (RES).

The echelon step sizes in z' and x' dimensions are represented by H and W respectively (see Fig. 1(c)). The temporal delay between the two neighboring beamlets is $2H/c$. This remain unchanged after the imaging system, whereas the transversal spacing between adjacent beamlets reduces from W to $f_2/f_1 W$. The PM condition given by Eq. (4).

$$\tan(\gamma) = 2Hf_1 / (Wn_g f_2) \quad (4)$$

It can be seen from Fig. 4(c1-c3) that the electric fields distributions are very similar to the CG scheme. However, the terahertz beam size is far larger ($\sim \times 2$) than the one produced by the CG.

Scheme (d): multi-step phase mask (MSPM).

In this scheme, no imaging system is required. The delay of each beamlet is generated by different propagation lengths inside the mask stripes. In the simulation, silica with refractive index of $n = 1.45$ [22] is chosen as the mask material due to its low dispersion at the OP wavelength. The phase mask step size in x' and z' dimensions are W and H respectively (see Fig. 1(d)). This scheme is very similar to the RES scheme. However, the imaging system in the RES scheme guarantees that at the image plane, each beamlet experiences the same condition. In this scheme, the diffraction modifies the beamlets envelope drastically, leading to poor terahertz electric field quality. It can be seen in the comparisons of Figs. 4(c1-c3) and 4(d1-d3) that an imaging system is necessary. This scheme can not outperform the RES scheme. The PM condition is given in Eq. (5).

$$\tan(\gamma) = (n - 1)H / (Wn_g) \quad (5)$$

Scheme (e): spatio-temporal chirp (STC).

In this scheme, no initial angular dispersion is present, leading to a maximum conversion efficiency among all 5 schemes discussed. However, the input OP pulse has to be broadband and a ELI-ALPS SYLOS laser can be an ideal option.

The full width half maximum (FWHM) of the overall input OP spectral bandwidth is presented in Eq. (6), which corresponds to a ~ 10 fs transform limited pulse. For a fair comparison, the local transform limited pulse duration (τ_0) at a given x' position is chosen to be 350 fs. Thus, the local pulse duration remains 500 fs after the chirp.

$$f_{\text{FWHM}} = \sigma'_x \sqrt{2 \log(2) (v^2 \tau^2 / 2 + 1 / \sigma_x'^2)} / \tau \pi \quad (6)$$

In Eq. (6), v is the spatial chirp rate and $\tau = \tau_0 / \sqrt{2 \log 2}$. The PM condition is presented in Eq. (7). The definition of OP as a function of ϕ_2 and v can be found in Eq. 19 of the supporting information.

$$\tan(\gamma) = v \phi_2 c / n_g \quad (7)$$

One can also choose a smaller input OP bandwidth together with a larger ϕ_2 . However, this leads to a temporal broadening of the OP at each spatial point, which is not in favor of the terahertz generation process.

With the given OP beam size ($\sigma'_x = 0.5$ mm), this scheme delivers the highest conversion efficiency and a spatially homogeneous few-cycle terahertz field. However, the disadvantage is that the input OP must contain a large bandwidth. Additionally, since the bandwidth of the OP is related to the input beam size (see Eq. (6)), this scheme is not applicable to large OP beam size.

5. Conclusion

Due to the non-collinear phase-matching, frequency down-shifted optical components generated via the second-order

effect, possess large angular spread. This leads to a spatial and temporal break-up of the optical pump, limiting the terahertz generation efficiency and reducing the few-cycle character of the generated terahertz fields. Additionally, large angular diffraction of the terahertz reduces the out-coupling efficiency of the terahertz fields which reduces the overall efficiency further. The simulations suggest that with lower OP input intensity, the terahertz electric field is closer to the single-cycle format along the x dimension and the terahertz beam size increases (see supporting information).

The CG and STC schemes form continuous TPF, where the PM condition is fulfilled along the entire transverse dimension. For the schemes related to beamlets (NLES, RES and MSPM), the entire beamlet-train forms the TPF with the required tilt angle. However, each individual beamlet itself has an offset with respect to the perfect TPF surface. Given a short interaction length, the discrete TPF schemes can not outperform the continuous TPF schemes in terms of efficiency. The MSPM scheme delivers the lowest efficiency and for large OP beam size, the efficiency is comparable to the RES scheme. We do not recommend MSPM scheme for small OP beam size. Among all 3 discrete TPF schemes, the NLES has the best performance in terms of efficiency and terahertz beam quality.

Schemes CG, NLES and RES, are applicable for a large range of parameters such as OP energy, bandwidth and beam size. Within these three schemes, the CG favors smaller interaction length (small beam size) and narrower OP bandwidth due to the large angular dispersion. NLES has a potential of delivering large and homogeneous terahertz beam because of the plan-parallel shape of the LN crystal and the smaller imaging errors in comparison to the CG scheme. Additionally, the generated terahertz spectrum does not depend on the OP beam size. The NLES and RES schemes require manufacturing μm sized structures, which is time consuming and prone to manufacturing errors.

Due to zero initial angular dispersion, the STC scheme delivers the highest conversion efficiency and spatially homogeneous few-cycle terahertz field. However, the OP pulse has to be broadband. Due to the spatial chirp, the bandwidth scales linearly with the OP beam size, making this scheme not applicable to large OP beam sizes.

Table 3 Comparison of different schemes. The symbols $\checkmark\checkmark$, \checkmark and \times represent recommend, neutral and not recommend respectively.

	(a) CG	(b) NLES	(c) RES	(d) STC	(e) MSPM
THz quality	\times	$\checkmark\checkmark$	\checkmark	$\checkmark\checkmark$	\times
σ'_x scalability	\checkmark	$\checkmark\checkmark$	\checkmark	\times	\checkmark
parameter flexibility	$\checkmark\checkmark$	\checkmark	$\checkmark\checkmark$	\checkmark	\times
efficiency	\checkmark	$\checkmark\checkmark$	\checkmark	$\checkmark\checkmark$	\times

A summary of the advantages and disadvantages of each scheme is listed in Table 3. Please note that the item " σ'_x scalability" is equivalent to large input OP energy since the

maximum fluence is limited by the damage threshold of the LN crystal.

Supporting Information

Supporting Information is available from the Wiley Online Library or from the author.

The code is available among reasonable request. To access the code, please contact (no space):

lu (dot) wangphysics (at) gmail (dot) com

Acknowledgments

Lu Wang would like to thank Dr. Dongfang Zhang for his inspiring discussions and patience, IMPRS for the support in both scientific research and in life and the rainy days in Hamburg for giving her no choice but to stay indoor and concentrate on research. György Tóth would like to thank the support of the János Bolyai Research Scholarship of the Hungarian Academy of Science. This project has received fundings from European Union's Seventh Framework Program (FP7/2007-2013) through the Synergy Grant AXSIS (609920) and the Hamburg Cluster of Excellence 'CUI: Advanced Imaging of Matter' of the Deutsche Forschungsgemeinschaft (DFG) - EXC 2056 - project ID 390715994.

Conflict of Interest

The authors declare no conflict of interest.

Keywords

terahertz generation, tilted-pulse-front, numerical modeling, phase-matching

References

- [1] P. Salén, M. Basini, S. Bonetti, J. Hebling, M. Krasilnikov, A. Y. Nikitin, G. Shamuilov, Z. Tibai, V. Zhaunerchyk, and V. Goryashko, *Physics Reports* (2019).
- [2] A. Davies, E. H. Linfield, and M. B. Johnston, *Physics in Medicine & Biology* **47**(21), 3679 (2002).
- [3] T. Kampfrath, A. Sell, G. Klatt, A. Pashkin, S. Mährlein, T. Dekorsy, M. Wolf, M. Fiebig, A. Leitenstorfer, and R. Huber, *Nature Photonics* **5**(1), 31–34 (2011).
- [4] O. Schubert, M. Hohenleutner, F. Langer, B. Urbaneck, C. Lange, U. Huttner, D. Golde, T. Meier, M. Kira, S. W. Koch, and R. Huber, *Nature Photonics* **8**(2), 119 (2014).
- [5] D. Zhang, A. Fallahi, M. Hemmer, X. Wu, M. Fakhari, Y. Hua, H. Cankaya, A. L. Calendron, L. E. Zapata, N. H. Matlis, and F. X. Kärtner, *Nature photonics* p. 1 (2018).
- [6] H. Bakker, S. Hunsche, and H. Kurz, *Physical review letters* **69**(19), 2823 (1992).

-
- [7] M. Hemmer, G. Cirimi, K. Ravi, F. Reichert, F. Ahr, L. Zapata, O. Mücke, A. L. Calendron, H. Çankaya, D. Schimpf et al., *Optics express* **26**(10), 12536–12546 (2018).
- [8] J. Hebling, *Optical and Quantum Electronics* **28**(12), 1759–1763 (1996).
- [9] J. Hebling, G. Almasi, I. Z. Kozma, and J. Kuhl, *Optics Express* **10**(21), 1161–1166 (2002).
- [10] S. Akturk, X. Gu, E. Zeek, and R. Trebino, *Optics express* **12**(19), 4399–4410 (2004).
- [11] B. K. Ofori-Okai, P. Sivarajah, W. R. Huang, and K. A. Nelson, *Optics express* **24**(5), 5057–5068 (2016).
- [12] Y. Avetisyan, A. Makaryan, V. Tadevosyan, and M. Tonouchi, *Journal of Infrared, Millimeter, and Terahertz Waves* **38**(12), 1439–1447 (2017).
- [13] L. Pálfalvi, G. Tóth, L. Tokodi, Z. Márton, J. A. Fülöp, G. Almási, and J. Hebling, *Optics express* **25**(24), 29560–29573 (2017).
- [14] P. S. Nugraha, G. Krizsán, C. Lombosi, L. Pálfalvi, G. Tóth, G. Almási, J. A. Fülöp, and J. Hebling, *Optics letters* **44**(4), 1023–1026 (2019).
- [15] L. Wang, T. Kroh, N. H. Matlis, and F. X. Kärtner, Full 3d+1 modelling of tilted-pulse-front setups for single-cycle terahertz generation, Manuscript submitted for publication, 2019.
- [16] L. Tokodi, J. Hebling, and L. Pálfalvi, *Journal of Infrared, Millimeter, and Terahertz Waves* **38**(1), 22–32 (2017).
- [17] J. Fülöp, L. Pálfalvi, S. Klingebiel, G. Almási, F. Krausz, S. Karsch, and J. Hebling, *Optics letters* **37**(4), 557–559 (2012).
- [18] K. Ravi, D. N. Schimpf, and F. X. Kärtner, *Optics express* **24**(22), 25582–25607 (2016).
- [19] M. Unferdorben, Z. Szaller, I. Hajdara, J. Hebling, and L. Pálfalvi, *Journal of Infrared, Millimeter, and Terahertz Waves* **36**(12), 1203–1209 (2015).
- [20] J. A. Fülöp, Z. Ollmann, C. Lombosi, C. Skrobol, S. Klingebiel, L. Pálfalvi, F. Krausz, S. Karsch, and J. Hebling, *Optics express* **22**(17), 20155–20163 (2014).
- [21] O. E. Martinez, *Optics communications* **59**(3), 229–232 (1986).
- [22] I. Malitson, *Josa* **55**(10), 1205–1209 (1965).